

# Time-Domain Characterization of Photonic Integrated Filters Subject to Fabrication Variations

Yinghao Ye <sup>1</sup>, Student Member, IEEE, Mi Wang, Student Member, IEEE, Domenico Spina <sup>2</sup>, Member, IEEE, Wim Bogaerts <sup>3</sup>, Senior Member, IEEE, and Tom Dhaene <sup>3</sup>, Senior Member, IEEE

**Abstract**—Fabrication variations are a key factor to degrade the performance of photonic integrated circuits (PICs), and especially wavelength filters. We propose an efficient modeling approach to quantify the effects of fabrication variations on the time-domain performance of linear passive photonic integrated circuits (including the wavelength filters) in the design stage, before fabrication. In particular, this novel approach conjugates the accuracy of the Polynomial Chaos (PC) expansion in describing stochastic variations and the efficiency of a Vector Fitting (VF)-based baseband modeling technique in performing time-domain simulations. A suitable example validates the performance of the proposed method.

**Index Terms**—Fabrication variations, photonic integrated circuits, polynomial Chaos, time-domain variability analysis.

## I. INTRODUCTION

**F**ABRICATION variations pose a considerable design challenge for silicon-on-insulator based *photonic integrated circuits* (PICs), since the high material index contrast makes photonic devices very sensitive to the geometry variations [1], [2]. Such variations normally lead to performance degradation of PICs after manufacturing and can even cause considerable yield loss. Hence, it is very important to quantify the performance variations of PICs before they are fabricated, which is often referred to as variability analysis and yield prediction. This is especially important in scenarios where the designer has no control over the fabrication process, which is becoming more common in the silicon photonics fabless/foundry ecosystem [3]. In this scenario, the Monte Carlo (MC) method is a robust, accurate and easy to implement solution. However, it is also very time consuming due to its slow convergence rate [4]. The Polynomial Chaos (PC) expansion is considered as an efficient alternative approach for variability analysis in electronic applications, for example

Manuscript received March 22, 2019; revised June 13, 2019; accepted July 23, 2019. Date of publication August 5, 2019; date of current version November 1, 2019. This work was supported in part by the Research Foundation-Flanders (FWO-Vlaanderen) under Grants G013815N and G056919N. (Corresponding author: Yinghao Ye.)

Y. Ye, D. Spina, and T. Dhaene are with the Internet Technology and Data Science Lab (IDLab), Department of Information Technology, Ghent University-imec, Ghent 9052, Belgium (e-mail: yinghao.ye@ugent.be; domenico.spina@ugent.be; tom.dhaene@ugent.be).

M. Wang and W. Bogaerts are with the Photonics Research Group, Department of Information Technology, and the Center for Nano- and Biophotonics (NB photonics), Ghent University-imec, Ghent 9052, Belgium (e-mail: mi.wang@ugent.be; wim.bogaerts@ugent.be).

Color versions of one or more of the figures in this paper are available online at <http://ieeexplore.ieee.org>.

Digital Object Identifier 10.1109/JLT.2019.2933311

in [5]–[10], and in recent years it has also been demonstrated on PICs [11]–[15]. In the latter case, however, the proposed techniques focus mainly on the variability analysis of suitable performance indicators defined in the wavelength/frequency domain, such as coupling coefficients [11], [12], 3-dB bandwidth [13], [14], transmission or scattering matrices [15]. It is also very important to perform *time-domain* variability analysis of linear and passive PICs, such as filters, which is a challenging task for complex PICs [2], [16]. In fact, from a system performance point of view, the time-domain performance for a given input signal, expressed as an eye diagram or constellation diagram, is a more direct and intuitive measure of the effect of the variations on signal integrity [17].

In this paper, we propose a time-domain variability analysis approach for passive photonic circuits under uncertainty effects, which is based on two recent techniques: PC-based macromodeling for characterizing the variations [6], [9], [15] and baseband modeling for efficient time-domain simulations [18], [19]. In particular, the PC-based macromodeling approach [9] leverages on the PC expansion of the scattering parameters of the circuits under stochastic effects, and employs the Galerkin projection method and the Vector Fitting (VF) algorithm to compute a deterministic, stable and passive state-space model describing the relation between the PC coefficients of the input and output signals of the circuits. This model is usually called “augmented”, since it has a higher number of ports than the original circuit under study [9]. Since a direct time-domain simulation of a state-space model computed at optical frequencies is time and memory consuming [18], [19], the augmented model is converted into an equivalent baseband representation, according to the technique introduced in [18], [19], thereby obtaining a baseband augmented model which can be efficiently simulated. Furthermore, pertinent time-domain statistical information of the circuit input/output signals can be computed by means of only one time-domain simulation of such model. In this paper we especially focus on wavelength filters, as they represent an important category of passive photonic circuits and their performance suffers severely from fabrication variations when they are not designed to be robust [20].

The paper is organized as follows. Section II describes the problem statement. Section III presents the standard MC approach for time-domain variability analysis, while Section IV proposes the novel PC-based approach. A detailed efficiency analysis of the proposed technique is presented in Section V, and a relevant application example is presented in Section VI,

where the proposed technique is compared to the MC analysis in terms of accuracy and efficiency. Conclusions are drawn in Section VII.

## II. PHOTONIC FILTERS SUBJECT TO FABRICATION VARIATIONS

Photonic filters are often studied in the frequency (or wave-length) domain, as their transfer function depends on suitable (geometrical or optical) design parameters and the frequency. Hence, it is straightforward to describe a photonic filter subject to fabrication variation via a scattering matrix  $S(f, \xi)$ , where  $f$  is the frequency and the vector  $\xi$  collects all the normalized random variables of the problem at hand, which represent the design parameters affected by fabrication variations (e.g. width and thickness of a waveguide, coupling coefficients, effective index). The port signals of the scattering matrix of the filter are incident and reflected waves, which have the relation

$$\mathbf{b}(f, \xi) = S(f, \xi)\mathbf{a}(f, \xi). \quad (1)$$

$S(f, \xi)$  is a  $N \times N$  matrix when the filter under study has  $N$  ports. Note that, due to the variability of the filter, no matter whether the incident waves are deterministic or stochastic, the reflected waves  $\mathbf{b}(f, \xi)$  will always depend on  $\xi$  and can be considered stochastic quantities. In general, the incident waves  $\mathbf{a}(f, \xi)$  can also be considered stochastic quantities. Indeed, even if the filter under study is connected to deterministic photonic components (not under stochastic effects) the stochastic outgoing waves  $\mathbf{b}(f, \xi)$  of the filter can result in reflections due to mismatch at the port joints, which are also stochastic and become the incident waves of the filter  $\mathbf{a}(f, \xi)$ . However, if the filter terminations are deterministic and port reflections can be neglected, the incident waves can be assumed deterministic.

The challenge addressed in this paper is to quantify the impact of the random parameters  $\xi$  on the port signals in the time domain.

## III. MONTE CARLO APPROACH

The MC method is the standard approach for such variability analysis. In our problem formulation, it requires the following three steps: 1) computing a large number of samples of the random variables  $\xi_i$  for  $i = 1, \dots, N_{MC}$ , according to their distribution. For each sample, the scattering parameters of the filter are calculated, representing  $N_{MC}$  different filters; 2) building models for all the  $N_{MC}$  filters and performing  $N_{MC}$  time-domain simulations to obtain the port signals; 3) computing the relevant statistics, such as mean, standard deviation, probability density function (PDF) or any other stochastic information of interest, based on the data collected so far.

In this framework, it is crucial to choose a suitable modeling approach for time-domain simulations, considering that a large number  $N_{MC}$  is required to accurately estimate the stochastic information [4]. In this paper, we adopt the baseband modeling technique proposed in [18], [19] for time-domain modeling and simulations, which is elaborated as follows.

For each filter with parameters  $\xi_i$ , the scattering matrix has to be evaluated at a set of frequencies in the range of interest, denoted by  $S(f_r, \xi_i)$  for  $r = 1, \dots, R$ . Then, a continuous VF

model can be built [21]

$$S(f, \xi_i) = \sum_{k=1}^K \frac{\mathbf{R}_k}{j2\pi f - p_k} + \mathbf{D}, \quad (2)$$

where  $\mathbf{R}_k$  are  $N \times N$  matrices containing the residues and  $p_k$  are the corresponding poles, which can be either real or complex conjugate pairs, while  $\mathbf{D}$  is a real matrix. Note that the model (2) is stable and passive: its stability is preserved by a pole-flipping scheme, while passivity assessment and enforcement can be accomplished by using robust standard techniques [22]–[24]. Next, a time-domain state-space model can be analytically derived from (2) [22]:

$$\begin{cases} \frac{d\mathbf{x}(t, \xi_i)}{dt} = \mathbf{A}\mathbf{x}(t, \xi_i) + \mathbf{B}\mathbf{a}(t, \xi_i) \\ \mathbf{b}(t, \xi_i) = \mathbf{C}\mathbf{x}(t, \xi_i) + \mathbf{D}\mathbf{a}(t, \xi_i), \end{cases} \quad (3)$$

where  $\mathbf{a}(t, \xi_i)$  and  $\mathbf{b}(t, \xi_i)$  are the time-domain counterparts of  $\mathbf{a}(f, \xi_i)$  and  $\mathbf{b}(f, \xi_i)$ , respectively, and  $\mathbf{x}(t, \xi_i)$  collects all the state variables.  $\mathbf{A}$ ,  $\mathbf{B}$ ,  $\mathbf{C}$ ,  $\mathbf{D}$  are the state-space matrices of  $S(f, \xi_i)$ . In particular,  $\mathbf{A}$  is a diagonal matrix with all the poles  $p_k$  as diagonal entries,  $\mathbf{B}$  is a matrix containing only ones and zeros,  $\mathbf{C}$  contains all the residues  $\mathbf{R}_k$ , while  $\mathbf{D}$  is the same as in (2).

The model (3) represents a system of first-order ordinary differential equations (ODE) that can be solved via robust numerical methods with respect to the incident waves  $\mathbf{a}(t, \xi_i)$ . However, the port signals  $\mathbf{a}(t, \xi_i)$  and  $\mathbf{b}(t, \xi_i)$  are modulated optical waves defined at the Terahertz frequency range, and a time-step on femtosecond-scale is needed to solve (3), which is impractical in terms of memory requirements and computational time [18], [19]. To address this challenge, baseband equivalents  $\mathbf{a}_B(t, \xi_i)$  for the optical waves  $\mathbf{a}(t, \xi_i)$  are defined [18]:

$$\mathbf{a}(t, \xi_i) = \Re[\mathbf{a}_B(t, \xi_i)e^{j2\pi f_c t}], \quad (4)$$

$$\mathcal{H}[\mathbf{a}(t, \xi_i)] = \Im[\mathbf{a}_B(t, \xi_i)e^{j2\pi f_c t}], \quad (5)$$

where  $\Re(\cdot)$  and  $\Im(\cdot)$  stand for the real and imaginary part, respectively, and  $\mathcal{H}(\cdot)$  represents the Hilbert transform. The signals  $\mathbf{a}_B(t, \xi_i)$  are called baseband equivalents since they no longer contain the fast oscillation of the optical carrier. Correspondingly, a baseband equivalent system for (3) was proposed in [18], [19]

$$\begin{cases} \frac{d\mathbf{x}_B(t, \xi_i)}{dt} = (\mathbf{A} - j2\pi f_c \mathbf{I})\mathbf{x}_B(t, \xi_i) + \mathbf{B}\mathbf{a}_B(t, \xi_i) \\ \mathbf{b}_B(t, \xi_i) = \mathbf{C}\mathbf{x}_B(t, \xi_i) + \mathbf{D}\mathbf{a}_B(t, \xi_i), \end{cases} \quad (6)$$

where  $\mathbf{a}_B(t, \xi_i)$ ,  $\mathbf{b}_B(t, \xi_i)$ , and  $\mathbf{x}_B(t, \xi_i)$  are the baseband equivalents of  $\mathbf{a}(t, \xi_i)$ ,  $\mathbf{b}(t, \xi_i)$ , and  $\mathbf{x}(t, \xi_i)$ , respectively.

Then, the system of ODE (6) can be solved efficiently with a much larger time step compared to (3), since the baseband equivalent signals have spectrum in the radio frequency (RF) band [18]. Note that for photonic circuits we are only interested in the baseband equivalent signals (e.g.  $\mathbf{b}_B(t, \xi_i)$ ) rather than the fast oscillating modulated optical signals (e.g.  $\mathbf{b}(t, \xi_i)$ ), since  $\mathbf{b}_B(t, \xi_i)$  represents the useful information that  $\mathbf{b}(t, \xi_i)$  carries [18], [25]. Furthermore, the optical signals can be analytically

calculated from their baseband counterpart, as shown in (4). Interested readers are referred to [18], [19] for more details about the baseband signals and models.

The MC analysis is completed by repeating this procedure for each sample  $\xi_i$  of the random variables and pertinent statistical analyses can be performed based on the large number of time-domain simulations performed.

#### IV. POLYNOMIAL CHAOS-BASED APPROACH

In contrast with the MC method, the technique described in this section is able to compute a statistical model of the input/output signals of the filter under study via a single time-domain simulation, which can be used to efficiently and accurately perform time-domain variability analysis, as described in the following.

##### A. PC-Based Augmented Systems

The PC expansion is an efficient modeling method to quantify stochastic variations. The main properties of the PC expansion and the procedure to build PC-based augmented systems are described in this section.

According to the PC theory, the stochastic quantities in (1) can be represented as [26], [27]:

$$\begin{aligned} \mathbf{S}(f_r, \xi) &\approx \sum_{m=0}^M \mathbf{S}_m(f_r) \varphi_m(\xi), \\ \mathbf{a}(f_r, \xi) &\approx \sum_{m=0}^M \mathbf{a}_m(f_r) \varphi_m(\xi), \\ \mathbf{b}(f_r, \xi) &\approx \sum_{m=0}^M \mathbf{b}_m(f_r) \varphi_m(\xi), \end{aligned} \quad (7)$$

where  $\varphi_m(\xi)$  are called basis functions, while  $\mathbf{S}_m(f_r)$ ,  $\mathbf{a}_m(f_r)$  and  $\mathbf{b}_m(f_r)$  for  $m = 0, \dots, M$  are suitable coefficients, referred to as PC coefficients. In particular, the basis functions  $\varphi_m(\xi)$  are orthonormal and depend on the joint distribution of the random variables  $\xi$  as

$$\langle \varphi_i(\xi), \varphi_m(\xi) \rangle = \int_{\Omega} \varphi_i(\xi) \varphi_m(\xi) W(\xi) d\xi = \delta_{im}, \quad (8)$$

where  $\delta_{im}$  is the Kronecker delta and  $\Omega$  represents the stochastic space where the random variables  $\xi$  are defined, while  $W(\xi)$  is a weight factor corresponding to the normalized joint probability density function of  $\xi$ .

Given (8), several techniques exist to estimate the basis functions [27]. It is important to note that, if the random variables  $\xi$  are independent, the basis functions are defined as product combination of the orthonormal polynomials corresponding to each *individual* random variable in  $\xi$ , which are *known* for certain distributions. For example,  $\varphi_m(\xi)$  are product of Hermite polynomials if the random variables  $\xi$  follow a Gaussian distribution, while for Uniform distribution they can be computed as product of Legendre polynomials [26], [27]. The accuracy of the approximations in (7) can be improved by increasing the number of basis functions  $M + 1$ , which depends on the

number  $Q$  of random variables in  $\xi$  and the PC order  $P$ :  $M + 1 = (Q + P)/(Q!P!)$  [26]. Since the basis functions are polynomials, the PC order  $P$  is defined as the maximum degree of the elements  $\varphi_m(\xi)$ , for  $m = 0, \dots, M$  [26], [27].

In this framework, only the PC coefficients must be estimated to obtain the models (7). Several non-intrusive techniques can be adopted to reach this goal, based on linear regression [15], numerical integration [26], or stochastic testing (ST) [5], [8]. Similar to the MC method, these approaches require to evaluate the filter scattering parameters for a set of samples  $N_{PC}$  of the random variables, with one main difference:  $N_{PC} \ll N_{MC}$ . Hence, computing the PC models (7) is much more efficient than performing a MC analysis.

Mathematically, the PC expansion process in (7) can be considered as projecting a stochastic quantity onto  $M + 1$  known orthonormal bases. In this work, the PC order  $P$  is selected according to the method in [28] and the PC coefficients are calculated via the ST technique [5], [8] to guarantee accurate PC expansions. Once the PC coefficients are calculated, the variability analysis can be performed with efficiency and accuracy:

- the mean and standard deviation of the stochastic quantity under study, for example  $\mathbf{S}(f_r, \xi)$ , can be directly calculated from the corresponding PC coefficients [26], [27];
- more complex stochastic moments, such as the probability density or the cumulative distribution function (CDF), can be estimated via a MC analysis based on the *analytical* models (7), which can be evaluated efficiently.

The interested reader is referred to [5], [7]–[15], [26], [27] for a complete description of the properties of the PC expansion, including its application to problems involving correlated random variables.

Now, by following the procedure described in [9], [15], it is possible to describe the relationship between the PC coefficients of the incident and reflected waves as:

$$\mathbf{b}_{PC}(f_r) = \mathbf{S}_{PC}(f_r) \mathbf{a}_{PC}(f_r), \quad (9)$$

where the vectors  $\mathbf{a}_{PC}(f_r)$  and  $\mathbf{b}_{PC}(f_r)$  are formed by the PC coefficients of the incident and reflected waves, respectively: they have a total of  $(M + 1)N$  elements. A detailed definition of  $\mathbf{a}_{PC}(f_r)$ ,  $\mathbf{b}_{PC}(f_r)$  and  $\mathbf{S}_{PC}(f_r)$  can be found in Appendix VII. Note that equation (9) is *deterministic*, since  $\mathbf{S}_{PC}(f_r)$  with size  $(M + 1)N \times (M + 1)N$  is obtained by a suitable combination of the PC coefficients  $\mathbf{S}_m(f_r)$  in (7) [9], [15]. It is important to remark that (9) describes a new system represented by  $\mathbf{S}_{PC}(f_r)$ , whose port signals are the PC coefficients of the incident and reflected waves of the original stochastic filter. In particular,  $\mathbf{S}_{PC}(f_r)$  is  $M + 1$  times larger than the original system under study in terms of ports number, and is often referred to as “augmented system” in the PC jargon. It is demonstrated in [9] that  $\mathbf{S}_{PC}(f_r)$  can be considered as a scattering matrix of a physical linear and passive system: it can be modeled with the same approaches that are used for modeling the filter (see (2)), as it will be described in the next section. Furthermore, an augmented matrix representation  $\mathbf{S}_{PC}(f_r)$  is adopted in [15] to model stochastic building blocks in PICs for efficient frequency-domain variability analysis.

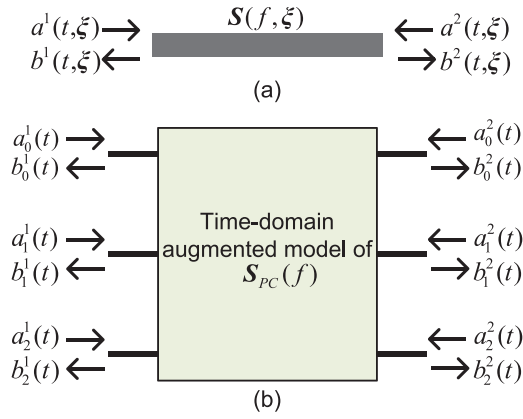


Fig. 1. (a) Waveguide under stochastic effects; (b) the corresponding time-domain augmented model.

Note that, when the incident waves do not depend on the random variables considered ( $\mathbf{a}(f_r, \boldsymbol{\xi}) = \mathbf{a}(f_r)$ ), equation (9) still holds and  $\mathbf{a}_{PC}(f_r) = [\mathbf{a}(f_r), \mathbf{0}, \mathbf{0}, \dots]^T$ , due to the properties of the PC expansion [26], [27].

### B. Time-Domain Augmented Model

Let us assume that  $\mathcal{S}_{PC}(f_r)$  has been computed for a discrete set of frequency values  $f_r$  for  $r = 1, \dots, R$ . Then, as it can be done for  $\mathcal{S}(f_r, \boldsymbol{\xi}_i)$ , a continuous frequency-dependent pole-residue model for  $\mathcal{S}_{PC}(f_r)$  can be built by means of the VF technique [21]

$$\mathcal{S}_{PC}(f) = \sum_{l=1}^L \frac{\mathbf{R}_l^{PC}}{j2\pi f - p_l^{PC}} + \mathbf{D}_{PC}, \quad (10)$$

where  $\mathbf{R}_l^{PC}$  are  $(M+1)N \times (M+1)N$  matrices containing the residues and  $p_l^{PC}$  are the poles, while  $\mathbf{D}_{PC}$  is a real matrix. Next, it is straightforward to convert (10) into a corresponding time-domain state-space representation [22]

$$\begin{cases} \frac{d\mathbf{x}_{PC}(t)}{dt} = \mathbf{A}_{PC}\mathbf{x}_{PC}(t) + \mathbf{B}_{PC}\mathbf{a}_{PC}(t) \\ \mathbf{b}_{PC}(t) = \mathbf{C}_{PC}\mathbf{x}_{PC}(t) + \mathbf{D}_{PC}\mathbf{a}_{PC}(t), \end{cases} \quad (11)$$

where  $\mathbf{A}_{PC}$ ,  $\mathbf{B}_{PC}$ ,  $\mathbf{C}_{PC}$ ,  $\mathbf{D}_{PC}$  are the state-space matrices of  $\mathcal{S}_{PC}(s)$  and can be directly calculated from (10) according to [22]. Note that  $\mathbf{x}_{PC}(t)$  is the corresponding state-vector, while  $\mathbf{a}_{PC}(t)$  and  $\mathbf{b}_{PC}(t)$  are the time-domain counterparts of  $\mathbf{a}_{PC}(f)$  and  $\mathbf{b}_{PC}(f)$ , respectively, which collect all the PC coefficients  $\mathbf{a}_m(t)$  of  $\mathbf{a}(t, \boldsymbol{\xi})$  and  $\mathbf{b}_m(t)$  of  $\mathbf{b}(t, \boldsymbol{\xi})$ .

To better understand this model, let us consider a waveguide in Fig. 1(a), which depends on one random variable (such as the width of the waveguide). If three basis functions are used for the PC expansion (PC order  $P = 2$ ), then the corresponding time-domain augmented model is shown in Fig. 1(b). In this case,  $\mathbf{a}_{PC}(t) = [a_0^1(t), a_0^2(t), a_1^1(t), a_1^2(t), a_2^1(t), a_2^2(t)]^T$ , where  $a_0^1(t)$  represents the first PC coefficient of the stochastic signal at port one and so on.

Now, time-domain simulations can be performed by solving the system of first-order ODE (11) with input signals  $\mathbf{a}_{PC}(t)$ . However, the PC coefficients collected in  $\mathbf{a}_{PC}(t)$  have spectrum in the terahertz frequency range, considering that the optical signals  $\mathbf{a}(t, \boldsymbol{\xi})$  are defined at such frequencies and the PC basis functions are time independent. As a result, similar to (3), time-domain simulations of (11) would have to adopt time steps of the order of the femtoseconds and would be very time and memory consuming [18]. This issue is addressed in the following by defining a baseband augmented model.

### C. Time-Domain Baseband Augmented Model

The PC expansion of  $\mathbf{a}(t, \boldsymbol{\xi})$  and its baseband equivalent  $\mathbf{a}_B(t, \boldsymbol{\xi})$  are

$$\mathbf{a}(t, \boldsymbol{\xi}) \approx \sum_{m=0}^M \mathbf{a}_m(t) \varphi_m(\boldsymbol{\xi}), \quad (12)$$

$$\mathbf{a}_B(t, \boldsymbol{\xi}) \approx \sum_{m=0}^M \mathbf{a}_{Bm}(t) \varphi_m(\boldsymbol{\xi}).$$

Combining (4) and (12), there is

$$\sum_{m=0}^M \mathbf{a}_m(t) \varphi_m(\boldsymbol{\xi}) = \Re \left[ \sum_{m=0}^M \mathbf{a}_{Bm}(t) \varphi_m(\boldsymbol{\xi}) e^{j2\pi f_c t} \right]. \quad (13)$$

Thanks to (8), projecting (13) on the  $i$ -th PC basis function via Galerkin projection gives [26]

$$\mathbf{a}_i(t) = \Re[\mathbf{a}_{Bi}(t) e^{j2\pi f_c t}], \quad (14)$$

which indicates that the PC coefficients  $\mathbf{a}_i(t)$  of the optical signals  $\mathbf{a}(t, \boldsymbol{\xi})$  can be analytically recovered from the PC coefficients  $\mathbf{a}_{Bi}(t)$  of the corresponding baseband equivalents  $\mathbf{a}_B(t, \boldsymbol{\xi})$ . Then, by collecting all the elements  $\mathbf{a}_i(t)$  and  $\mathbf{a}_{Bi}(t)$  in vectors, it leads to:

$$\mathbf{a}_{PC}(t) = \Re[\mathbf{a}_{BPC}(t) e^{j2\pi f_c t}]. \quad (15)$$

Starting from (5) and (12), the following relation can be obtained in the same way

$$\mathcal{H}[\mathbf{a}_{PC}(t)] = \Im[\mathbf{a}_{BPC}(t) e^{j2\pi f_c t}]. \quad (16)$$

It is easy to prove that similar relations also hold for  $\mathbf{b}_{PC}(t)$  and  $\mathbf{x}_{PC}(t)$  in (11).

Hence, considering the relations (15) and (16), a baseband augmented model for (11) can be derived by following the same procedure used for the filter (see (3) and (6)) [18], which leads to:

$$\begin{cases} \frac{d\mathbf{x}_{BPC}(t)}{dt} = (\mathbf{A}_{PC} - j2\pi f_c \mathbf{I})\mathbf{x}_{BPC}(t) + \mathbf{B}_{PC}\mathbf{a}_{BPC}(t) \\ \mathbf{b}_{BPC}(t) = \mathbf{C}_{PC}\mathbf{x}_{BPC}(t) + \mathbf{D}_{PC}\mathbf{a}_{BPC}(t). \end{cases} \quad (17)$$

Now, all the PC coefficients  $\mathbf{b}_{BPC}(t)$  of the stochastic baseband equivalent signals  $\mathbf{b}_B(t, \boldsymbol{\xi})$  can be obtained by performing only a *single* time-domain simulation of (17) in the baseband with efficiency and accuracy. With these PC coefficients, the mean and standard deviation of the baseband port signals can

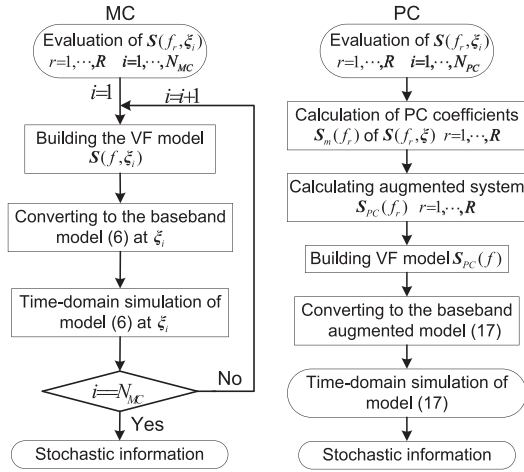


Fig. 2. Flowchart of the MC approach (left) and the proposed PC-based method (right).

be immediately calculated, while a cheap MC analysis based on the obtained PC model can also be performed to estimate more complex quantities, such as the PDF, eye or constellation diagrams [26], [27]. Note that, starting from the PC coefficients of the baseband signals, it is possible to analytically estimate the corresponding PC coefficients of the signals at optical frequencies, see (15): the variations of the optical signals are fully characterized by the PC model of their baseband counterpart.

The key steps of the MC method presented in Section III and of the novel PC-based approach are illustrated in Fig. 2. It is important to remark that both techniques start with evaluating scattering matrices, whereas the MC and PC-based approach require  $N_{MC}$  and  $N_{PC}$  samples respectively, and  $N_{PC}$  is much smaller than  $N_{MC}$ , as will be demonstrated in Section VI. Note that several steps in the MC approach have to be repeated  $N_{MC}$  times, while those in PC-based approach need to be carried out only once. These differences make the proposed method far superior in terms of efficiency.

## V. EFFICIENCY ANALYSIS OF THE PROPOSED PC-BASED APPROACH

The proposed modeling framework, shown in Fig. 2, offers a high degree of flexibility and can be applied to a large range of passive photonic circuits. In particular, different non-intrusive PC techniques can be adopted to compute the PC coefficients of the scattering parameters of the system under study, and the baseband augmented model can be simulated in many ODE solvers. In the following, a detailed breakdown of the computational cost of the proposed method will be presented, where the different factors influencing the modeling efficiency will be discussed.

The starting point of the proposed technique is the calculation of the PC model of the scattering parameters of the system under study: the scattering parameters must be evaluated over a set of points in the stochastic space  $\xi_i$  for  $i = 1, \dots, N_{PC}$ . The sampling strategy depends on the specific non-intrusive method used to compute the PC coefficients, such as linear regression, numerical integration [26], [27], or ST-based techniques [5], [8]: for example, by using the ST-based technique leads to

$N_{PC} = M + 1$ , where  $M + 1$  depends on the number  $Q$  of random variables and PC order  $P$ . Next, for each sample in the stochastic space, the scattering parameters can be evaluated via conventional simulations (e.g. with an electromagnetic solver or circuit simulator), and the computational cost is influenced by the size of one such simulation and the number of frequency samples considered. Note that, the sampling strategy in the frequency domain depends only on the accurate description of the circuit behavior in the chosen frequency range: any existing sampling technique valid for deterministic systems can be adopted (i.e. equally spaced linear/logarithmic sampling or adaptive sampling methods). Now, the desired augmented system  $S_{PC}(f_r)$  can be computed for all the frequency values  $f_r$  considered [9], [15].

Next, a stable and passive state-space model (11) of the augmented system  $S_{PC}(f_r)$  can be computed via the VF algorithm, whose computational cost depends on the size of the system, the number of poles needed in the pole-residue model (10) [21] and the specific passivity assessment and enforcement algorithms used among the ones presented in the literature, such as [22]–[24]. For example, the passivity enforcement via the approach in [23] has a computational complexity of  $O(L^3 N^3)$ , where  $L$  is the number of poles and  $N$  the number of ports of the system under study.

Finally, time-domain simulations are carried out by solving the system of first-order ODE (17) with baseband input signals. When the Matlab routine *lsim* is employed to solve the ODE, the computational complexity of the two main steps in *lsim* are  $O(J^3)$  and  $O(J^2 N_t)$  [29], respectively, where  $J$  is the size of  $\mathbf{A}_{PC}$  and  $N_t$  is the total number of time samples.

Therefore, the efficiency of the proposed technique is sensitive to the number of random variables. More random variables leads to more basis functions for the same PC order (see Section IV-A), which has two effects: not only the number  $N_{PC}$  of samples required to calculate the PC coefficients of the filter scattering parameters increases, but also the size of  $S_{PC}(f_r)$  and its corresponding baseband model increases as well, which can reduce the efficiency of the proposed method in both the model building and simulation phases. This is a de facto challenge for PC-based techniques: their efficiency is high if the number of random variables is (relatively) limited [27]. A possible solution to reduce such modeling complexity is to adopt sparse PC expansion [30], [31], leading to augmented matrices with a high degree of sparsity [9]. Indeed, for a given PC order  $P$ , it is possible that only a subset of all the basis functions computed via the formula  $M + 1 = (Q + P)! / (Q! P!)$  is sufficient to achieve an accurate estimation of the variability of the system under study [30], [31].

## VI. STUDY OF A RING-LOADED MZI FILTER UNDER STOCHASTIC EFFECTS

This section presents an application example of the proposed modeling and simulation techniques. The scattering parameters of the photonic filter under study are evaluated via the *Caphe* circuit simulator (Luceda Photonics), while the baseband augmented model calculation and the time-domain simulations are carried out in Matlab on a personal computer with Intel Core

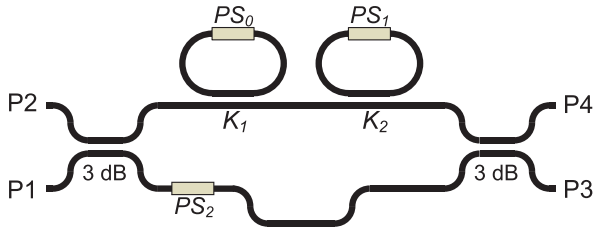


Fig. 3. Structure of the ring-loaded MZI filter under study.

i3 processor and 8 GB RAM. Note that the VF technique that is available at [32] is adopted in this work.

#### A. Ring-Loaded MZI Filter With Four Random Variables

The proposed technique is applied to a compact silicon-on-insulator bandpass filter presented in [33], whose structure is shown in Fig. 3. The filter is designed based on unbalanced Mach-Zehnder interferometer (MZI) loaded with a pair of ring resonators (RR). The length of the unloaded arm is set in such a way that the free spectral range of the RR matches that of the MZI. The characteristics of the filter, such as 3 dB bandwidth, off-band rejection and shape factor, are mainly determined by the phase delays  $PS_0$ ,  $PS_1$ ,  $PS_2$  of the three phase shifters, and power coupling coefficients  $K_1$ ,  $K_2$  of the two directional couplers, as indicated in Fig. 3. In particular,  $K_1$  and  $K_2$  affect the bandwidth tunability and off-band rejection; the phase difference between  $PS_0$  and  $PS_1$  has an impact on the 3 dB bandwidth; the condition  $PS_2 = m\pi + (PS_0 + PS_1)/2$  has to be satisfied in order to achieve a symmetric passband with regard to the center frequency, where  $m$  is an integer [33]. In our design, these parameters are chosen as  $PS_0 = 0$ ,  $PS_1 = \pi$ ,  $PS_2 = \pi/2$ ,  $K_1 = 0.67$ ,  $K_2 = 0.67$ .

We assume that, due to fabrication variations, the coupling coefficients  $K_1$  and  $K_2$  vary independently from chip to chip and can be represented as Gaussian random variables with standard variation of 0.02. The phase shifters are implemented by diode-loaded heaters, and their phase delays can be tuned by controlling the electric power applied to the resistance load. However, in practice, it is very challenging to set and keep the phase delay to an exact value, since the control accuracy suffers from electrical and thermal crosstalk and variations in the nonlinear power-phase response. As a result, the phase delays can be considered as random variables unless very sophisticated control scheme is used (e.g. [34], [35]). In this work, we assume that  $PS_1$  and  $PS_2$  are independent Gaussian distributed random variables with a standard deviation of two degrees while the phase shifter with phase delay  $PS_0$  is not operating since it is zero. Hence, the filter scattering parameters depend on  $Q = 4$  random variables. Note that physical parameters, such as the width and thickness of waveguides, can also be assumed as random variables in the proposed modeling framework, since the modeling approach leverages on non-intrusive PC expansion [26], [27].

To build the baseband augmented model, first a suitable modeling frequency range around the carrier frequency

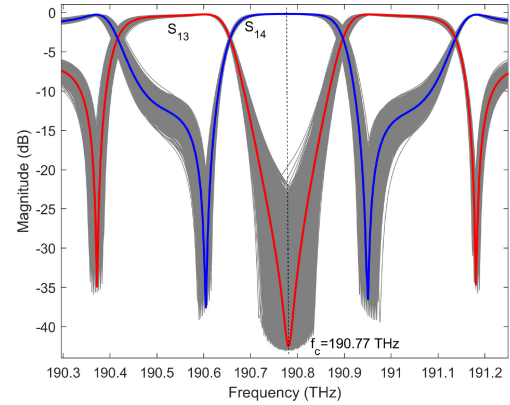


Fig. 4. The variation (gray lines) in frequency response of the filter due to stochastic effects and the nominal design (red  $S_{13}$  and blue  $S_{14}$ ).

$f_c = 190.77$  THz must be defined: [190.29; 191.25] THz. This choice depends on the spectrum of the modulated input signals: a bandwidth of  $\pm 480$  GHz is sufficient for our application. In particular, 260 frequency samples that are uniformly distributed over the modeling frequency range are adopted. Then, a PC order  $P = 2$  is chosen according to the method in [28], leading to 15 basis functions, which is sufficient to obtain an accurate PC expansion of the scattering parameters in this case. According to the ST approach [5], only  $N_{PC} = 15$  samples of  $\xi$  are chosen in the stochastic space, where  $S(f_r, \xi_i)$  for  $i = 1, \dots, N_{PC}$  are evaluated. Next, the PC coefficients of the scattering matrices  $S(f_r, \xi)$  are computed by a linear regression approach [8]. Finally, the obtained PC coefficients  $S_m(f_r)$  for  $r = 1, \dots, 260$  are used to calculate  $S_{PC}(f_r)$ , as described in Section IV-A.

With the VF technique [21], [22], [24], a stable, passive, and continuous state-space model  $S_{PC}(f)$  in the form (11) is built with 34 poles [9], [10]. The magnitude of the maximum absolute error between the VF model and the data is less than  $-55$  dB. It is important to remark that the PC coefficients  $S_m(f)$  can always be estimated from the corresponding augmented system  $S_{PC}(f)$  [9], [10]. Since a continuous frequency-domain model of  $S_{PC}(f)$  has been computed via the VF technique, the PC coefficients of the filter scattering matrix can be evaluated at any frequency point in the frequency range considered, which is [190.29; 191.25] THz in this case. Hence, a cheap MC analysis based on the PC model of the scattering parameters is conducted to calculate  $S(f_k, \xi_i)$  for  $i = 1, \dots, 10000$  and  $k = 1, \dots, 800$ , as shown in Fig. 4.

The blue and red curve are the frequency response with the intended design parameters (also called nominal design), while the gray lines represent the variations in the frequency response of the filter under stochastic effects. Note that the carrier frequency is chosen at the passband center of the filter as indicated in Fig. 4. Finally, the baseband stochastic model can be built according to (17) for efficient time-domain variability analysis.

We assume that the filter is excited at port P1 with quadrature amplitude modulated (QAM) source signal, then the incident waves are  $a(t, \xi) = a(t)$ , while the outputs  $b(t, \xi)$  will vary

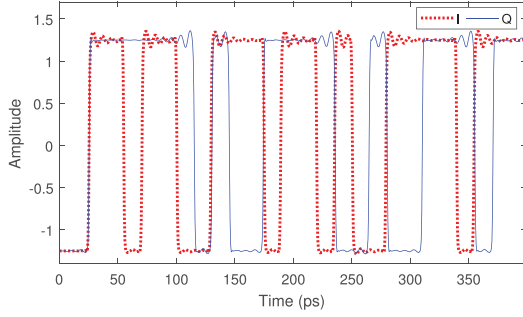


Fig. 5. The in-phase part (I) and quadrature part (Q) of the input QAM signal.

from chip to chip due to the variations of  $PS_1$ ,  $PS_2$ ,  $K_1$  and  $K_2$ . The in-phase part  $I(t)$  and quadrature part  $Q(t)$  of the QAM input signal are pseudo-random sequence of 1000 bits with a bit time of 15 ps, whose first 25 bits are plotted in Fig. 5. Note that  $I(t)$  and  $Q(t)$  correspond to the real and imaginary parts of the baseband equivalent of the QAM modulated signal, respectively [18]. Furthermore, any input signal with a generic shape can be adopted here as the filter excitation, as long as the chosen modeling frequency range covers the spectrum of the signal.

Considering that the incident waves at port P1 is a deterministic source signal, its first PC coefficient is equal to the source signal itself, while all the others are zeros (see Section IV-A). Similarly, we assume that the other ports have no incident waves, so their PC coefficients are all zeros. In this framework, the input signal for the built baseband model (17) can be easily calculated:  $\mathbf{a}_{BPC}(t) = [I(t) + jQ(t), 0, 0, \dots]$ . It is important to remark that in this example only the port P1 is excited for an easier demonstration of the simulation results. In fact, the proposed modeling and simulation technique allows that all the ports are excited at the same time with different input signals. Once we have the baseband augmented model and its input  $\mathbf{a}_{BPC}(t)$ , time-domain simulations can be conducted by solving the first-order ODE (17) by robust ODE solvers [18]. In this work, the Matlab linear system simulator *lsim* is adopted. Finally, all the PC coefficients of the baseband reflected wave  $\mathbf{b}_B(t, \xi)$  are obtained, which are collected in the output  $\mathbf{b}_{BPC}(t)$ . The mean and standard deviation (sigma) of the output signal  $\mathbf{b}_B(t, \xi)$  are readily calculated from  $\mathbf{b}_{BPC}(t)$  [9], [10].

As a benchmark, a time-domain MC analysis is also performed with  $N_{MC} = 10000$  samples of  $PS_1$ ,  $PS_2$ ,  $K_1$  and  $K_2$ , by following the procedure outlined in Section III. Fig. 6 shows the *mean* and *mean*  $\pm$  *3sigma* of the output at P3 and P4 at the first 200 ps, computed via the proposed PC-based approach and via the MC analysis: an excellent agreement can be observed.

Furthermore,  $\mathbf{b}_{BPC}(t)$  is a cheap but accurate PC model, from which the stochastic moments of  $\mathbf{b}(t, \xi)$ , such as mean, standard deviation, PDF and CDF, can be efficiently computed. Indeed, when the PDF of  $\mathbf{b}_B(t, \xi)$  are desired, a cheap MC analysis based on the obtained PC model can be immediately conducted [9], [10], [15]. In this example, a MC analysis of the constellation diagrams of the output at port P4 is carried out by computing  $\mathbf{b}_B(t, \xi_i)$  of the filters at 10000 samples of  $\xi$ . Note that the real and imaginary parts of  $\mathbf{b}_B(t, \xi_i)$  are the in-phase part  $I(t)$  and

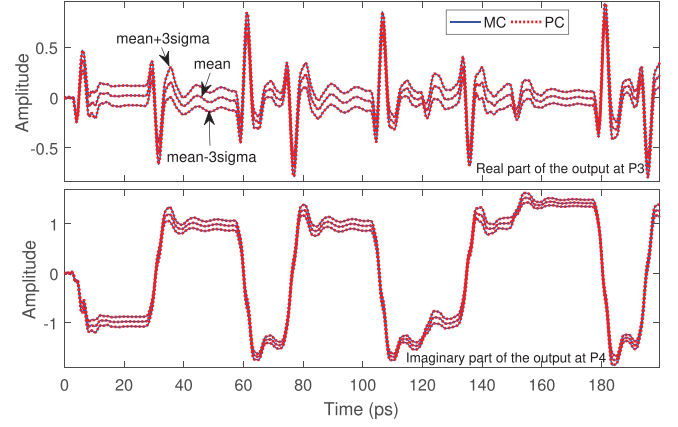


Fig. 6. Variations of the output at port P3 and P4 obtained from the proposed technique (red dotted line) and MC analysis (blue line).

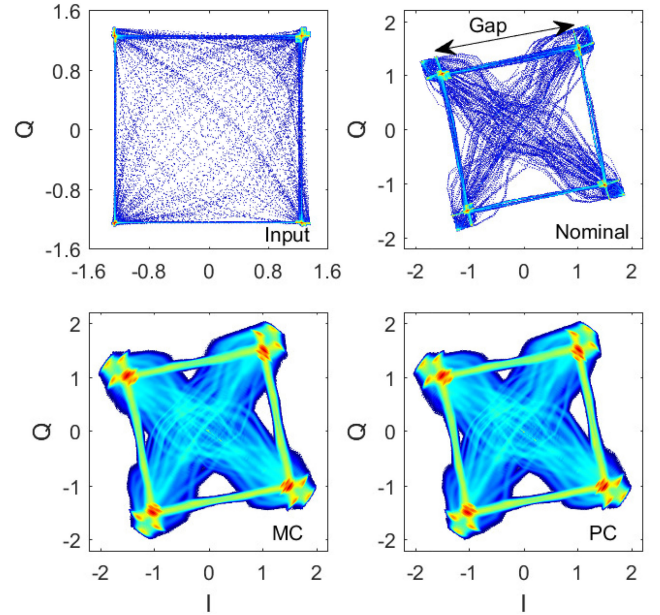


Fig. 7. Constellation diagrams of: input (top left), the output at P4 of nominal design (top right), 10000 filters from MC analysis described in Section III (bottom left), and 10000 filters from the computed PC model (bottom right).

quadrature part  $Q(t)$ , respectively [18], and the constellation diagram can be immediately plotted with  $I(t)$  and  $Q(t)$ . Fig. 7 shows the 10000 diagrams computed from the cheap PC model and MC analysis, and the diagrams for input signal and output signal of the nominal design for comparison. Again, the results demonstrate the accuracy of the proposed method.

The computational time for the proposed technique and MC analysis are compared in Table I in term of three phases: evaluating scattering matrices, building the models with the VF technique, and time-domain simulations. It demonstrates that the proposed technique is much more efficient than the MC method, while achieving a comparable accuracy.

To study how the variations in  $PS_1$ ,  $PS_2$ ,  $K_1$  and  $K_2$  impact the output signal at port P4, the standard deviation for ( $K_1$ ,  $K_2$ )

TABLE I  
EFFICIENCY OF THE PROPOSED TECHNIQUE

Technique	Steps	Computational time
Proposed technique	Extract scattering matrices at 15 $(PS_1, PS_2, K_1, K_2)$ samples	1 min 2 s
	Build baseband augmented model (17)	1 min 52 s
	Time-domain simulation	9 min 22 s
	Total time	12 min 16 s
MC	Extract scattering matrices at 10000 $(PS_1, PS_2, K_1, K_2)$ samples	11 h 35 min
	Build 10000 baseband models (6)	1 h 54 min
	10000 time-domain simulations	1 h 56 min
	Total time	15 h 25 min

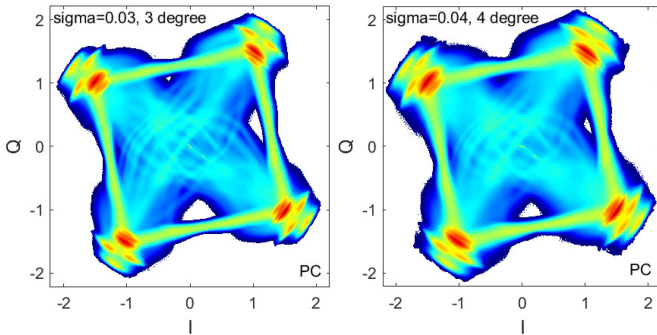


Fig. 8. Constellation diagrams of 10000 filters from the proposed PC-based technique when different variations are considered.

and  $(PS_1, PS_2)$  is first increased to 0.03 and 3 degrees, respectively, then to 0.04 and 4 degrees, respectively. Performing the variability analysis via the MC approach outlined in Section III is particularly expensive, since a new set of  $N_{MC} = 10000$  samples must be evaluated each time the standard deviation of the random variables changes. With the proposed technique, only  $N_{PC} = 15$  samples of the random parameters need to be computed anew for the chosen standard deviation values, which leads to a great efficiency gain. The effect of the change in the standard deviation on the constellation diagrams by means of the proposed method is shown in Fig. 8.

Furthermore, the PDF of the constellation symbol gap can also be calculated from both the MC analysis and the proposed PC-based technique, as illustrated in Fig. 9. Note that the gap is defined as the distance between the centers of two constellation symbols, as indicated in Fig. 7. It is evident that the PDF of the gap obtained from both techniques show an excellent agreement for the original assumption of the standard deviations. When the standard deviations increase, a clear larger spread of the gap distribution can be observed from the PDF computed via the efficient PC-based technique.

### B. Ring-Loaded MZI Filter With Six Random Variables

To study the efficiency of the proposed technique with regard to the number of random variables, besides the four random variables in Section VI-A, we also consider the power coupling coefficients of the two 3 dB directional couplers in Fig. 3 as random variables with mean value 0.5 and standard deviation

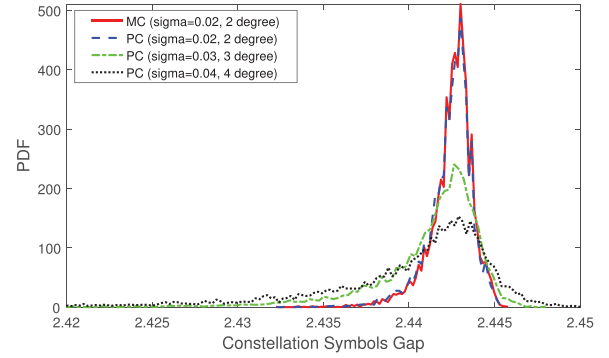


Fig. 9. PDF of the constellation symbols gap calculated from MC analysis and the proposed PC-based technique while considering different variations.

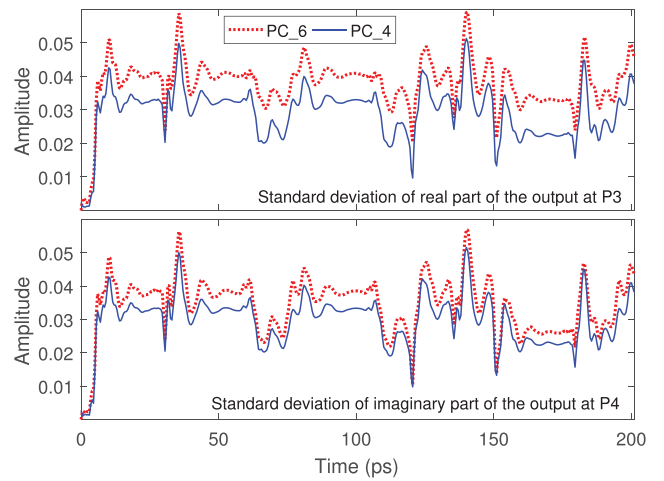


Fig. 10. Standard deviations of the outputs of the filter with four random variables and six random variables, which are obtained by the proposed PC-based technique.

0.01. Hence, a total of six random variables is considered in this example.

Following the same steps in Section VI-A, first a PC order  $P = 2$  is selected via the method in [28]. Note that the number of basis functions becomes 28 with  $Q = 6$  random variables, which is almost doubled compared to the number of basis functions in Section VI-A. Then, with the ST technique,  $N_{PC} = 28$  samples of  $\mathcal{S}(f_r, \xi_i)$  for  $i = 1, \dots, N_{PC}$  are evaluated to calculate PC coefficients via a linear regression approach [8]. Next,  $\mathcal{S}_{PC}(f_r)$  is computed and has a size of  $112 \times 112$ , since  $(M + 1)N = 112$ , while the size of  $\mathcal{S}_{PC}(f_r)$  in Section VI-A is  $60 \times 60$ . Note that  $\mathcal{S}_{PC}(f_r)$  are highly sparse matrices [9], [15]. A stable and passive state-space model (11) of  $\mathcal{S}_{PC}(f_r)$  can be built with 35 poles via the VF technique, while the magnitude of the maximum absolute error between the VF model and the data is less than  $-55$  dB. Finally the corresponding baseband augmented model in the form (17) is calculated from the VF model (11), as described in Section IV-C. With the same input signals used in Section VI-A, time-domain simulations are performed via the ODE solver *lsim* in Matlab. Fig. 10 shows the standard deviations of the output signals calculated with the proposed PC-based technique, which is compared to the standard deviations of the same output signals in Section VI-A.

As far as the computational efficiency is concerned when the number of random variables increases to six, evaluating the scattering parameters  $\mathcal{S}(f_r, \xi_i)$  for  $i = 1, \dots, 28$  and  $r = 1, \dots, 260$  takes 2 min, building the baseband augmented model (17) requires 4 min 11 s, while 41 min 3 s are needed for time-domain simulations. The total computational time is 47 min 14 s, which is about four times of the computational time in Section VI-A. However, the proposed approach is still significantly more efficient than the MC simulation with 10000 samples, achieving a speed-up of about  $20\times$ . One possible solution to reduce the impact of the number of random parameters on the efficiency of the proposed method is to adopt sparse PC expansions [30], [31], as indicated in Section V.

## VII. CONCLUSION

In this work, we presented an efficient baseband augmented modeling technique for time-domain variability analysis of photonic filters under stochastic effects. The proposed approach is applicable to general linear passive photonic devices and circuits, since it is based on the scattering parameters representation, and allows for an efficient characterization of the impact of random variables on the time-domain performance of photonic circuits. The accuracy and efficiency of the proposed method was validated by means of a comparison with the time-domain MC approach for a pertinent example of a photonic integrated filter circuit.

### APPENDIX A

#### DEFINITION OF THE AUGMENTED SYSTEMS

A detailed derivation of the augmented systems in Section IV-A can be found in [9], [15]. In this appendix, the definition of the port signals and the transfer function of a PC-based augmented systems is presented.

First, the port signals  $\mathbf{a}_{PC}(f_r)$ ,  $\mathbf{b}_{PC}(f_r)$  of the augmented systems are defined as

$$\mathbf{a}_{PC}(f_r) = \begin{bmatrix} \mathbf{a}_0(f_r) \\ \mathbf{a}_1(f_r) \\ \vdots \\ \mathbf{a}_M(f_r) \end{bmatrix}, \mathbf{b}_{PC}(f_r) = \begin{bmatrix} \mathbf{b}_0(f_r) \\ \mathbf{b}_1(f_r) \\ \vdots \\ \mathbf{b}_M(f_r) \end{bmatrix}, \quad (18)$$

where  $\mathbf{a}_m(f_r)$  and  $\mathbf{b}_m(f_r)$  are the  $m$ -th PC coefficients of  $\mathbf{a}(f_r, \xi)$  and  $\mathbf{b}(f_r, \xi)$ , respectively, which are defined in (7). In particular,  $\mathbf{a}_m(f_r)$  and  $\mathbf{b}_m(f_r)$  can be expressed as

$$\mathbf{a}_m(f_r) = \begin{bmatrix} a_m^1(f_r) \\ a_m^2(f_r) \\ \vdots \\ a_m^N(f_r) \end{bmatrix}, \mathbf{b}_m(f_r) = \begin{bmatrix} b_m^1(f_r) \\ b_m^2(f_r) \\ \vdots \\ b_m^N(f_r) \end{bmatrix}, \quad (19)$$

where  $a_m^1(f_r)$  indicates the  $m$ -th PC coefficient of the first port signal  $a^1(f_r, \xi)$  in  $\mathbf{a}(f_r, \xi)$ , while  $\mathbf{a}(f_r, \xi) = [a^1(f_r, \xi), a^2(f_r, \xi), \dots, a^N(f_r, \xi)]^T$ . The time-domain counterparts  $\mathbf{a}_{PC}(t)$ ,  $\mathbf{b}_{PC}(t)$  are defined in a similar way.

The scattering parameters of the augmented system  $\mathcal{S}_{PC}(f_r)$  can be obtained by a suitable combination of the PC coefficients  $\mathcal{S}_m(f_r)$  in (7) as [9], [15]

$$[\mathcal{S}_{PC}(f_r)]_{ij} = \sum_{m=0}^M \mathcal{S}_m(f_r) \langle \varphi_m(\xi) \varphi_j(\xi), \varphi_i(\xi) \rangle, \quad (20)$$

where

$$\langle \varphi_m(\xi) \varphi_j(\xi), \varphi_i(\xi) \rangle = \int_{\Omega} \varphi_m(\xi) \varphi_j(\xi) \varphi_i(\xi) W(\xi) d\xi. \quad (21)$$

Note that the integrals in (21) are frequency-independent and can be calculated upfront analytically or via numerical techniques [9], [15].

## REFERENCES

- [1] A. Waqas, D. Melati, and A. Melloni, "Sensitivity analysis and uncertainty mitigation of photonic integrated circuits," *J. Lightw. Technol.*, vol. 35, no. 17, pp. 3713–3721, Sep. 2017.
- [2] W. Bogaerts and L. Chrostowski, "Silicon photonics circuit design: Methods, tools and challenges," *Laser Photon Rev.*, vol. 12, no. 4, Mar. 2018, Art. no. 1700237.
- [3] U. Khan, Y. Xing, Y. Ye, and W. Bogaerts, "Photonic circuit design in a foundry+fabless ecosystem," *IEEE J. Sel. Topics Quantum Electron.*, vol. 25, no. 5, pp. 1–14, Sep. 2019.
- [4] G. Fishman, *Monte Carlo: Concepts, Algorithms, and Applications*. New York, NY, USA: Springer, 2013.
- [5] Z. Zhang, T. A. El-Moselhy, I. M. Elfadel, and L. Daniel, "Stochastic testing method for transistor-level uncertainty quantification based on generalized polynomial chaos," *IEEE Trans. Comput.-Aided Des. Integr. Circuits Syst.*, vol. 32, no. 10, pp. 1533–1545, Oct. 2013.
- [6] P. Manfredi, D. V. Ginste, D. De Zutter, and F. G. Canavero, "Uncertainty assessment of lossy and dispersive lines in spice-type environments," *IEEE Trans. Compon. Packag. Manuf. Technol.*, vol. 3, no. 7, pp. 1252–1258, Jul. 2013.
- [7] P. Manfredi and F. G. Canavero, "Efficient statistical simulation of microwave devices via stochastic testing-based circuit equivalents of nonlinear components," *IEEE Trans. Microw. Theory Techn.*, vol. 63, no. 5, pp. 1502–1511, May 2015.
- [8] P. Manfredi, D. V. Ginste, D. De Zutter, and F. G. Canavero, "Generalized decoupled polynomial chaos for nonlinear circuits with many random parameters," *IEEE Microw. Wireless Compon. Lett.*, vol. 25, no. 8, pp. 505–507, Aug. 2015.
- [9] D. Spina, T. Dhaene, L. Knockaert, and G. Antonini, "Polynomial chaos-based macromodeling of general linear multiport systems for time-domain analysis," *IEEE Trans. Microw. Theory Techn.*, vol. 65, no. 5, pp. 1422–1433, May 2017.
- [10] Y. Ye, D. Spina, P. Manfredi, D. V. Ginste, and T. Dhaene, "A comprehensive and modular stochastic modeling framework for the variability-aware assessment of signal integrity in high-speed links," *IEEE Trans. Electromagn. Compat.*, vol. 60, no. 2, pp. 459–467, Apr. 2018.
- [11] T. W. Weng, Z. Zhang, Z. Su, Y. Marzouk, A. Melloni, and L. Daniel, "Uncertainty quantification of silicon photonic devices with correlated and non-Gaussian random parameters," *Opt. Express*, vol. 23, no. 4, pp. 4242–4254, Feb. 2015.
- [12] Y. Xing, D. Spina, A. Li, T. Dhaene, and W. Bogaerts, "Stochastic collocation for device-level variability analysis in integrated photonics," *Photon. Res.*, vol. 4, no. 2, pp. 93–100, Apr. 2016.
- [13] T. W. Weng *et al.*, "Stochastic simulation and robust design optimization of integrated photonic filters," *Nanophotonics*, vol. 6, no. 1, pp. 299–308, 2017.
- [14] C. Cui and Z. Zhang, "Uncertainty quantification of electronic and photonic ICs with non-Gaussian correlated process variations," in *Proc. IEEE/ACM Int. Conf. Comput.-Aided Des.*, San Diego, CA, USA, Nov. 2018, pp. 1–8.
- [15] A. Waqas, D. Melati, P. Manfredi, and A. Melloni, "Stochastic process design kits for photonic circuits based on polynomial chaos augmented macro-modelling," *Opt. Express*, vol. 26, no. 5, pp. 5894–5907, Mar. 2018.

- [16] W. Bogaerts, Y. Xing, and U. Khan, "Layout-aware variability analysis, yield prediction, and optimization in photonic integrated circuits," *IEEE J. Sel. Topics Quantum Electron.*, vol. 25, no. 5, pp. 1–13, Sep. 2019.
- [17] M. Heins *et al.*, "Design flow automation for silicon photonics: Challenges, collaboration, and standardization," in *Proc. Silicon Photon. III, Syst. Appl.*, 2016, pp. 99–156.
- [18] Y. Ye, D. Spina, Y. Xing, W. Bogaerts, and T. Dhaene, "Numerical modeling of linear photonic system for accurate and efficient time-domain simulations," *Photon. Res.*, vol. 6, no. 6, pp. 560–573, Jun. 2018.
- [19] Y. Ye, D. Spina, W. Bogaerts, and T. Dhaene, "Baseband macromodeling of linear photonic circuits for time-domain simulations," *J. Lightw. Technol.*, vol. 37, no. 4, pp. 1364–1373, Feb. 2019.
- [20] P. De Heyn *et al.*, "Fabrication-tolerant four-channel wavelength-division-multiplexing filter based on collectively tuned Si microrings," *J. Lightw. Technol.*, vol. 31, no. 16, pp. 2785–2792, Aug. 2013.
- [21] B. Gustavsen and A. Semlyen, "Rational approximation of frequency domain responses by vector fitting," *IEEE Trans. Power Del.*, vol. 14, no. 3, pp. 1052–1061, Jul. 1999.
- [22] B. Gustavsen and A. Semlyen, "Fast passivity assessment for S-parameter rational models via a half-size test matrix," *IEEE Trans. Microw. Theory Techn.*, vol. 56, no. 12, pp. 2701–2708, Dec. 2008.
- [23] B. Gustavsen, "Fast passivity enforcement for pole-residue models by perturbation of residue matrix eigenvalues," *IEEE Trans. Power Del.*, vol. 23, no. 4, pp. 2278–2285, Oct. 2008.
- [24] D. Deschrijver and T. Dhaene, "Fast passivity enforcement of S-parameter macromodels by pole perturbation," *IEEE Trans. Microw. Theory Techn.*, vol. 57, no. 3, pp. 620–626, Mar. 2009.
- [25] C. Sorace-Agaskar, J. Leu, M. R. Watts, and V. Stojanovic, "Electro-optical co-simulation for integrated CMOS photonic circuits with VerilogA," *Opt. Express*, vol. 23, no. 21, pp. 27 180–27 203, Oct. 2015.
- [26] M. S. Eldred, "Recent advance in non-intrusive polynomial-chaos and stochastic collocation methods for uncertainty analysis and design," in *Proc. 50th AIAA/ASME/ASCE/AHS/ASC Struct., Struct. Dyn., Mater. Conf.*, Palm Springs, CA, USA, May 2009, pp. 2274:1–2274:37.
- [27] A. Kaintura, T. Dhaene, and D. Spina, "Review of polynomial chaos-based methods for uncertainty quantification in modern integrated circuits," *Electronics*, vol. 7, no. 3, 2018, pp. 30:1–30:21.
- [28] D. Spina, F. Ferranti, T. Dhaene, L. Knockaert, and G. Antonini, "Polynomial chaos-based macromodeling of multiport systems using an input-output approach," *Int. J. Numer. Model.*, vol. 28, no. 5, pp. 562–581, Sep./Oct. 2015.
- [29] K. Sou and O. L. De Weck, "Fast time-domain simulation for large-order linear time-invariant state space systems," *Int. J. Numer. Method Eng.*, vol. 63, no. 5, pp. 681–708, Mar. 2005.
- [30] G. Blatman and B. Sudret, "Adaptive sparse polynomial chaos expansion based on least angle regression," *J. Comput. Phys.*, vol. 230, no. 6, pp. 2345–2367, 2011.
- [31] J. Peng, J. Hampton, and A. Doostan, "A weighted  $\ell_1$ -minimization approach for sparse polynomial chaos expansions," *J. Comput. Phys.*, vol. 267, pp. 92–111, 2014.
- [32] 2009. [Online]. Available: [www.sintef.no/projectweb/vectfit/](http://www.sintef.no/projectweb/vectfit/)
- [33] P. Orlandi, F. Morichetti, M. J. Strain, M. Sorel, P. Bassi, and A. Melloni, "Photonic integrated filter with widely tunable bandwidth," *J. Lightw. Technol.*, vol. 32, no. 5, pp. 897–907, Mar. 2014.
- [34] A. Ribeiro and W. Bogaerts, "Digitally controlled multiplexed silicon photonics phase shifter using heaters with integrated diodes," *Opt. Express*, vol. 25, no. 24, pp. 29 778–29 787, Nov. 2017.
- [35] M. Milanizadeh, D. Aguiar, A. Melloni, and F. Morichetti, "Canceling thermal cross-talk effects in photonic integrated circuits," *J. Lightw. Technol.*, vol. 37, no. 4, pp. 1325–1332, Feb. 2019.